

# **Estimating the Feasibility of Probing the Epoch of Reionization with the 21cm-Ly $\alpha$ Cross-Power Spectrum**

Prepared for:

Drs. Daniel Jacobs (Director), Judd Bowman, & Alex Van Engelen

Arizona State University

School of Earth and Space Exploration

Prepared By:

Tyler Cox

Arizona State University

School of Earth and Space Exploration

Astrophysics Senior Thesis

December 5<sup>th</sup>, 2019

## Abstract

One of the primary goals of astrophysics is the observation of the Epoch of Reionization. The Epoch of Reionization (EoR) is a period in the history of the universe when during which the first luminous sources (stars, galaxies, etc.) formed and ionized the neutral gas. Despite best efforts of observations of this period, the process by which the universe transitioned from neutral to ionized is still largely a mystery. Next-generation reionization-era experiments such as the Hydrogen of Epoch of Reionization Array (HERA) and the Spectro-Photometer for the History of the Universe, Epoch of Reionization, and Ices Explorer (SPHEREx) look to independently probe the EoR by mapping the intensity of 21 cm and Lyman- $\alpha$  fluctuations respectively. While each instrument promises sensitivity not yet seen with this kind of measurement, the presence of bright radio foregrounds 4-5 orders of magnitude larger than the 21 cm fluctuations HERA seeks to measure and low-redshift H $\alpha$  interlopers. Cross-correlation of these signals looks to be a promising way to reduce measurement systematics from each instrument and provide an independent confirmation on the progression of reionization. In this paper, I present an estimation of the feasibility of tracing the evolution of reionization using the 21 cm-Ly $\alpha$  cross-power spectrum as measured by HERA and SPHEREx. Using the reionization modeling code, 21cmFAST, I simulate the evolution of the EoR. I show that HERA and SPHEREx have the ability to measure the cross-power spectrum at large scales given. In future work, this technique will be used to put constraints on astrophysical parameters.

- EoR
- 21cm Measurement and Difficulties
- Ly $\alpha$  Measurement and Difficulties
- Cross-Correlation
- Results
- Future Work

# Contents

<b>I. Contents</b>	<b>ii</b>
<b>II. List of Figures</b>	<b>iii</b>
<b>1 Introduction</b>	<b>1</b>
1.1 The Early Universe . . . . .	1
1.2 The Epoch of Reionization . . . . .	2
1.3 Synergies Between Experiments . . . . .	2
1.3.1 The Hydrogen Epoch of Reionization Array . . . . .	2
1.3.2 SPHEREx: an All-Sky Spectral Survey . . . . .	2
<b>2. Modeling 21 cm and Ly<math>\alpha</math> Fluctuations</b>	<b>4</b>
2.1. 21 cm Fluctuations . . . . .	5
2.2. Ly $\alpha$ Fluctuations . . . . .	6
2.2.1 Ly $\alpha$ Emitters . . . . .	7
2.2.2 Ionized IGM . . . . .	8
2.2.3 Ly $\alpha$ Attenuation . . . . .	10
<b>3. Cross-Correlation Studies</b>	<b>11</b>
3.1. Cross-Power Spectrum . . . . .	11
3.2. Observational Uncertainties . . . . .	11
3.3. Foreground Contamination . . . . .	13
<b>4. Conclusions</b>	<b>17</b>
<b>References</b>	<b>21</b>
<b>Appendix</b>	<b>23</b>

# List of Figures

1.	Epoch of Reionization Timeline . . . . .	2
2.	Spin-Flip Transition of Neutral Hydrogen . . . . .	2
3.	Upper Limits on Reionization . . . . .	3
4.	Redshift and Resolution Coverage of Intensity Mapping Experiments . . . . .	4
5.	HERA Image and Layout . . . . .	5
6.	SPHEREx Instrument . . . . .	6
7.	Simulated 21cm and Ly $\alpha$ emission . . . . .	9
8.	21 cm Power Spectrum . . . . .	12
9.	Ly $\alpha$ Power Spectrum . . . . .	13
10.	21 cm-Ly $\alpha$ Cross-Power Spectrum . . . . .	14
11.	Cross-Correlation Coefficient . . . . .	15
12.	Cross-Power Spectrum Error Budget . . . . .	17
13.	Foreground Wedge . . . . .	18
14.	Optimistic vs. Moderate Foreground Treatment . . . . .	19
15.	Cross-Power Spectrum Signal-to-Noise . . . . .	20

## Acknowledgements

First and foremost, I would like to thank my research advisors had since I've been a part of the Low-Frequency Cosmology Lab (in no particular order), Adam Beardsley, Judd Bowman, and Danny Jacobs. I am incredibly grateful for the opportunities that you've provided and the guidance that you've given.

Thank you to my third committee member, Alex Van Engelen, for enthusiastically agreeing to sit on my committee despite the late notice.

I would also like to thank my friends, fellow students, and colleagues, who have made my time at ASU as enjoyable as it has been. In particular, I would like to thank Shane Bechtel, Lily Whitler and Samuel Nigh for their support and friendship. I would also like to thank Lindsay Berkhouit, Mrudula , Steven Murray, and Matt Kolopanis and all of the members of the Low-Frequency Cosmology Lab for making my time here successful and

Finally, I would like to thank my family for their constant encouragement and support. I can't thank you enough.

# 1 Introduction

## 1.1 The Early Universe

Immediately following the Big Bang, the Universe was primarily composed of a hot plasma of fundamental particles. In its early state, it was much too hot and dense to form the atoms that form the complex structures the astronomers observe today. Photons that were emitted during this early period scattered off free particles, leaving the Universe opaque to electromagnetic radiation. This lasted until roughly 400,000 years after the Big Bang, at which time the Universe had expanded and cooled sufficiently for electrons to bind to atomic nuclei forming the first atoms of Hydrogen and Helium. Once formed, photons were able to freely propagate through the intergalactic medium (IGM) as cosmic microwave background radiation.

The Cosmic Microwave Background (CMB) is arguably the best studied cosmological period in the history of the universe. Space-based observatories such as WMAP and Planck have measured the CMB with increasing accuracy giving cosmologists insight to the very first fractions of a second after the Big Bang.

Much of the history of the Universe after  $\sim$ 1 billion years the Big Bang is observable as well. Optical and infrared observatories such as those done with the Hubble Space Telescope (HST) allows astronomers to regularly observe redshift galaxies out to  $z \sim 4$ , while a number of objects at  $z > 7$  have been observed with gravitational lensing. While some objects have been observed at high redshifts, little is known about the period of cosmological time

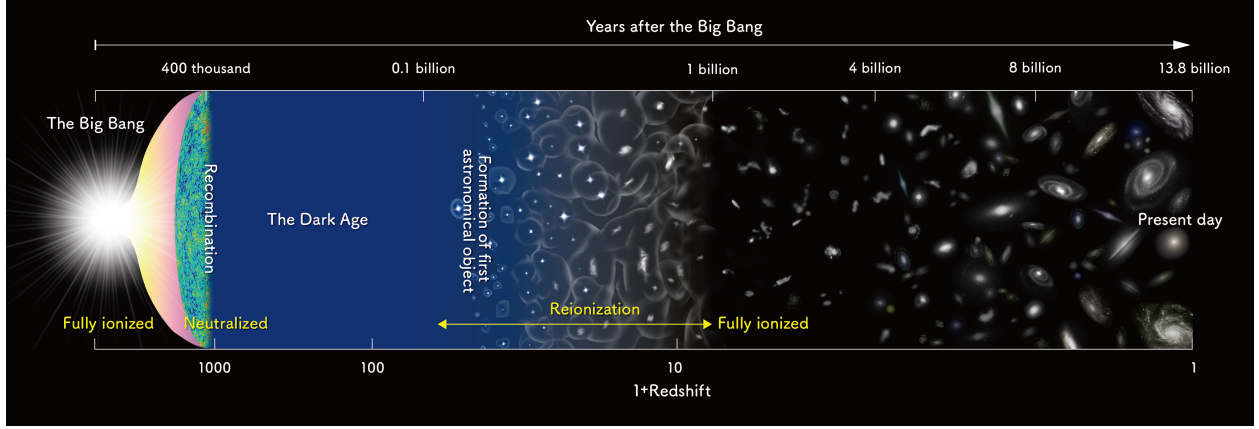


**Figure 1.** Timeline of the history of the universe from its formation (left) to present day (right).

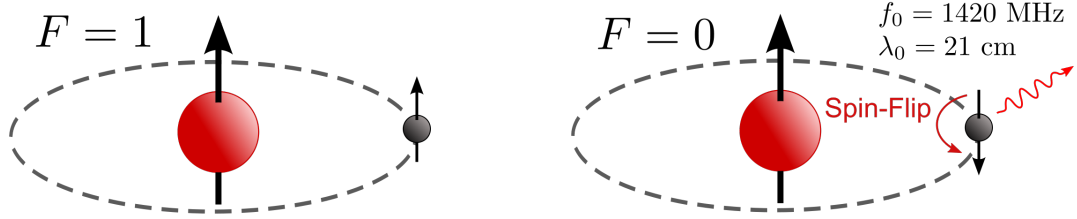


**Figure 2.** A depiction of the spin-flip transition of neutral hydrogen. Initially, the spin of the proton and electron are parallel and oriented in the same direction. The transition occurs when the electron's spin spontaneously flips from the higher energy parallel alignment to the lower energy anti-parallel alignment, releasing a photon with a wavelength of 21 cm.

between when the.

## 1.2 The Epoch of Reionization

### 1.3 Synergies Between Experiments

Intensity mapping is a way of understanding the large scale behavior of a thing.

#### 1.3.1 The Hydrogen Epoch of Reionization Array

HERA DeBoer et al. (2017)

#### 1.3.2 SPHEREx: an All-Sky Spectral Survey

The Spectro-Photometer for the History of the Universe, Epoch of Reionization, and Ices Explorer (SPHEREx), is a next-generation instrument that will do blank. SPHEREx looks

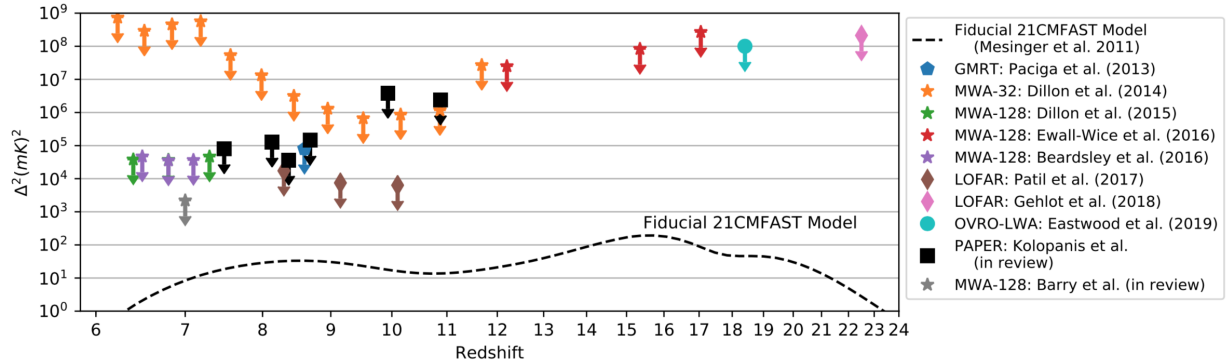


**Figure 3.** A summary of the upper limits on the 21 cm power spectrum across reionization. Plotted in the dashed line is a fiducial model of the 21 cm power spectrum as simulated by 21CMFAST. Image taken from [Liu & Shaw \(2019\)](#)

at things! Doré et al. (2014)

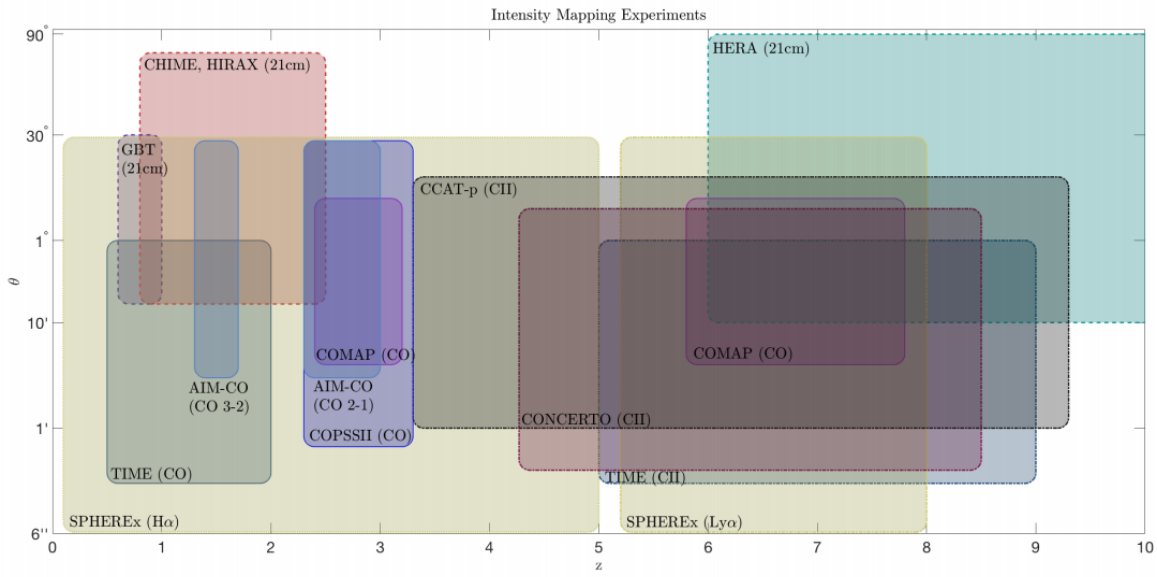


**Figure 4.** A figure representing the resolution, field of view, and redshift range of upcoming intensity mapping experiments.

## 2. Modeling 21 cm and Ly $\alpha$ Fluctuations

In this section, I will discuss the effort to model the 21 cm and Ly $\alpha$  cosmological signals that will be used for cross-correlation later in this work. A significant amount of research has gone into the modeling effort of both 21 cm and Ly $\alpha$  fluctuations during the Epoch of Reionization.

While N-body and radiative transfer codes and analytic models accurately capture the physics of the evolution of galaxies and the IGM at small scales. Semi-numerical simulators on the other hand are much more computationally efficient at modeling the large-scale evolution of the IGM throughout the process of reionization. For this work, I use the semi-numerical simulator of the cosmological 21 cm signal, 21cmFAST [Mesinger et al. \(2011\)](#), to

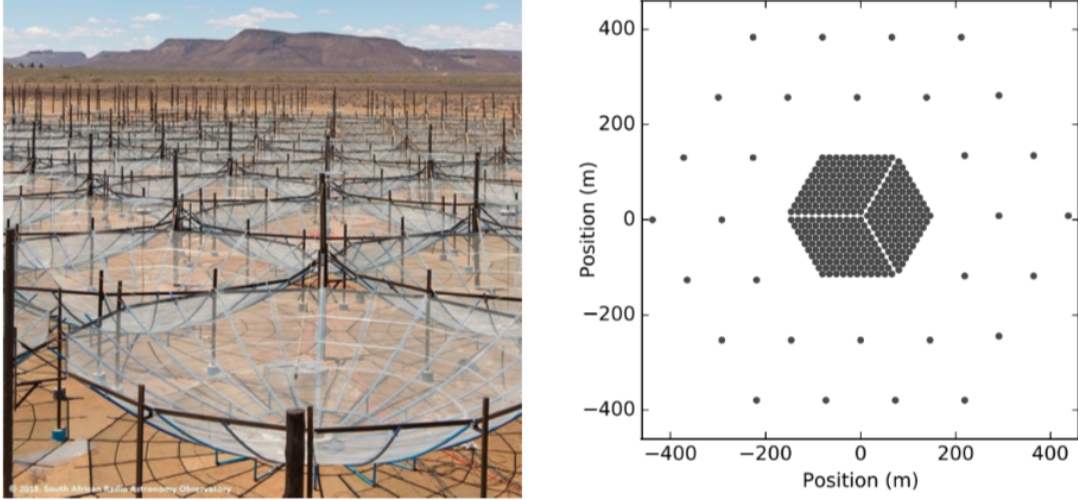


**Figure 5.** Left: An image of HERA as of late 2017. Right: A map of the full layout of HERA. The final array will contain a total of 350 dishes: 320 of which will be tightly packed hexagonal pattern with an additional 30 placed outside for increased imaging resolution

generate the 21 cm signal.

### 2.1. 21 cm Fluctuations

In the equation above,  $T_S$  is the gas spin temperature,  $T_\gamma$  is the CMB temperature,  $\tau_{\nu_0}$  is the optical depth at 21cm frequency,  $\delta_{\text{nl}}$  is the non-linear density contrast  $\delta_{\text{nl}} = \rho/\rho - 1$ ,  $H(z)$  is the Hubble parameter,  $dv_r/dr$  is the comoving gradient of the line of sight component of the comoving velocity, where all quantities are evaluated at redshift  $z = \nu_0/\nu - 1$ .

$$\begin{aligned} \delta T_b(z) &= \frac{T_S - T_\gamma}{1+z} \left(1 - e^{-\tau_{\nu_0}}\right) \\ &\approx 27x_{\text{HI}}(1 + \delta_{\text{nl}}) \left(\frac{H}{dv_r/dv + H}\right) \left(1 - \frac{T_\gamma}{T_S}\right) \\ &\quad \times \left(\frac{1+z}{10} \frac{0.15}{\Omega_M h^2}\right)^{1/2} \left(\frac{\Omega_b h^2}{0.023}\right) \text{ mK}, \end{aligned} \quad (1)$$

In the equation above,  $T_S$  is the gas spin temperature,  $T_\gamma$  is the CMB temperature,  $\tau_{\nu_0}$

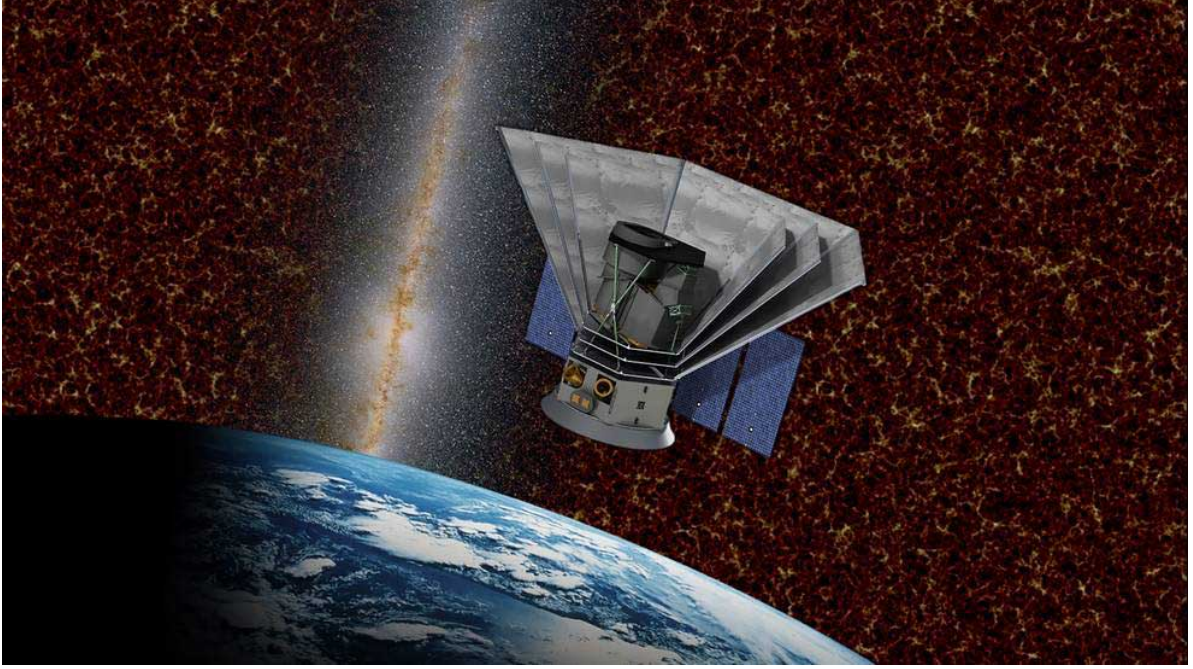


**Figure 6.** Simulated image of the SPHEREx probe in orbit.

is the optical depth at 21cm frequency,  $\delta_{\text{nl}}$  is the non-linear density contrast  $\delta_{\text{nl}} = \rho/\bar{\rho}_0 - 1$ ,  $H(z)$  is the Hubble parameter,  $dv_r/dr$  is the comoving gradient of the line of sight component of the comoving velocity, where all quantities are evaluated at redshift  $z = \nu_0/\nu - 1$ .

$$\delta_{21}(\mathbf{x}, z) = \frac{\delta T_b(\mathbf{x}, z)}{\delta \bar{T}_b(z)} - 1 \quad (2)$$

where  $\delta \bar{T}$  is the spatial average of the 21cm brightness temperature offset  $\delta T(\mathbf{x}, z)$ . The-  
her

## 2.2. Ly $\alpha$ Fluctuations

Here I will describe the parameterization of Ly $\alpha$  emission during reionization. I adopt the technique developed in Silva et al. (2013) and applied in Heneka et al. (2017). While modeling Ly $\alpha$  I focus two locations from which Ly $\alpha$  emission originates.

1. *Ly $\alpha$  Emitters (LAE):* This is emission that originates from within the virial radius Ly $\alpha$ -emitting galaxies themselves. The dominate components that contribute to emission within these galaxies are hydrogen recombinations and collisional excitation.

2. *Ionized Intergalactic Medium (IGM)*: This is emission that stems from the bubble of ionized gas that surround Ly $\alpha$ emitting galaxies. In these ionized bubbles, X-ray/UV heating and scattering of Lyman-n photons as well as recombinations of ionized hydrogen are the dominate contributors to Ly $\alpha$  emission.

### 2.2.1 Ly $\alpha$ Emitters

$$L_{\text{rec}}^{\text{gal}}(M, z) = E_{\text{Ly}\alpha} \dot{N}_{\text{Ly}\alpha}(M, z) \quad (3)$$

$$\dot{N}_{\text{Ly}\alpha}(M, z) = A_{\text{He}} \dot{N}_{\text{ion}} f_{\text{rec}} f_{\text{Ly}\alpha} [1 - f_{\text{esc}}(M, z)] \quad (4)$$

Here  $A_{\text{He}} = (4 - Y_{\text{He}}) / (4 - 3Y_{\text{He}})$ . I also assume  $f_{\text{rec}} \approx 0.66$

$$f_{\text{Ly}\alpha} = C_{\text{dust}} \times 10^{-3} (1 + z)^{\zeta} \quad (5)$$

Here  $C_{\text{dust}}$  and  $\zeta$  are fit for in.

$$f_{\text{esc}}(M, z) = \exp [\alpha(z) M^{\beta(z)}] \quad (6)$$

Here  $\alpha$  and  $\beta$  are redshift dependent parameters defined in

$$\text{SFR} = 2.8 \times 10^{-28} \left( \frac{M}{M_{\odot}} \right)^a \left( 1 + \frac{M}{c_1} \right)^b \left( 1 + \frac{M}{c_2} \right)^d [M_{\odot} \text{ yr}^{-1}] \quad (7)$$

Where  $a = -0.94$ ,  $b = -1.7$ ,  $c_1 = 10^9 M_{\odot}$ ,  $c_2 = 7 \times 10^{10} M_{\odot}$ , and  $d = -1.7$  which fitted parameters defined in (SFR PAPER). Here are more relations  $\dot{N}_{\text{ion}} = Q_{\text{ion}} \times \text{SFR}(M, z)$  where  $Q_{\text{ion}} \approx 5.8 \times 10^{60} M_{\odot}^{-1}$ .

$$L_{\text{exc}}^{\text{gal}}(M, z) = f_{\text{exc}} E_{\text{exc}} \dot{N}_{\text{ion}} \quad (8)$$

Also  $E_{\text{exc}} \approx 2.14 \text{ eV}$ .

$$I_{\nu}^{\text{gal}}(\mathbf{x}, z) = y(z) d_A^2(z) \frac{L^{\text{gal}}(\mathbf{x}, z)}{4\pi d_L^2} \quad (9)$$

Here  $d_A$  is the comoving angular diameter distance,  $d_L$  is the luminosity distance, and  $y(z) = \lambda_0(1+z)^2 / H(z)$  (for the rest-frame wavelength of Ly $\alpha$  radiation,  $\lambda_0 = 1216 \text{ \AA}$ ).

$$\bar{I}_{\nu} = \int_{M_{\min}}^{M_{\max}} dM \frac{dn}{dM} I_{\nu}^{\text{gal}}(M, z) \quad (10)$$

The relation above is used to define an average intensity at a given redshift. Here  $dn/dm$  is the Tormen-Sheth halo mass function,  $M_{\min} = 10^8 M_{\odot}$ , and  $M_{\max} = 10^{13} M_{\odot}$ . The halo mass function acts as a weight in a weighted average.

### 2.2.2 Ionized IGM

Diffuse

$$l_{\text{rec}} = E_{\text{Ly}\alpha} f_{\text{rec}} \dot{n}_{\text{rec}}(\mathbf{x}, z) \quad (11)$$

$$\dot{n}_{\text{rec}}(\mathbf{x}, z) = \alpha_A n_e(z) n_{HII}(z) \quad (12)$$

This is an equation  $n_e = x_i(\mathbf{x}, z) n_b(\mathbf{x}, z)$  and

$$n_b(\mathbf{x}, z) = \bar{n}_{b,0} (1+z)^3 [1 + \delta_{\text{nl}}(\mathbf{x}, z)] \quad (13)$$

Where  $1 + \delta_{\text{nl}}(\mathbf{x}, z)$  is the non-linear density contrast.

$$\alpha_A \approx 4.2 \times 10^{-13} \left( T_K / 10^4 \text{ K} \right)^{-0.7} (1+z)^3 \left[ \text{cm}^3 \text{ s}^{-1} \right] \quad (14)$$

$$I_{\text{rec}, \nu} = y(z) d_A^2(z) \frac{l_{\text{rec}}(\mathbf{x}, z)}{4\pi d_L^2(z)} \quad (15)$$

Scattered

$$I_\nu = \frac{6E_{\text{Ly}\alpha} d_A^2(z)}{(1+z)^2 d_L^2(z)} J_\alpha(\mathbf{x}, z) \quad (16)$$

$$\delta I_\nu(\mathbf{x}, z) = \sum_i \frac{\nu I_{\nu,i}(\mathbf{x}, z)}{\nu \bar{I}_\nu(z)} - 1 \quad (17)$$

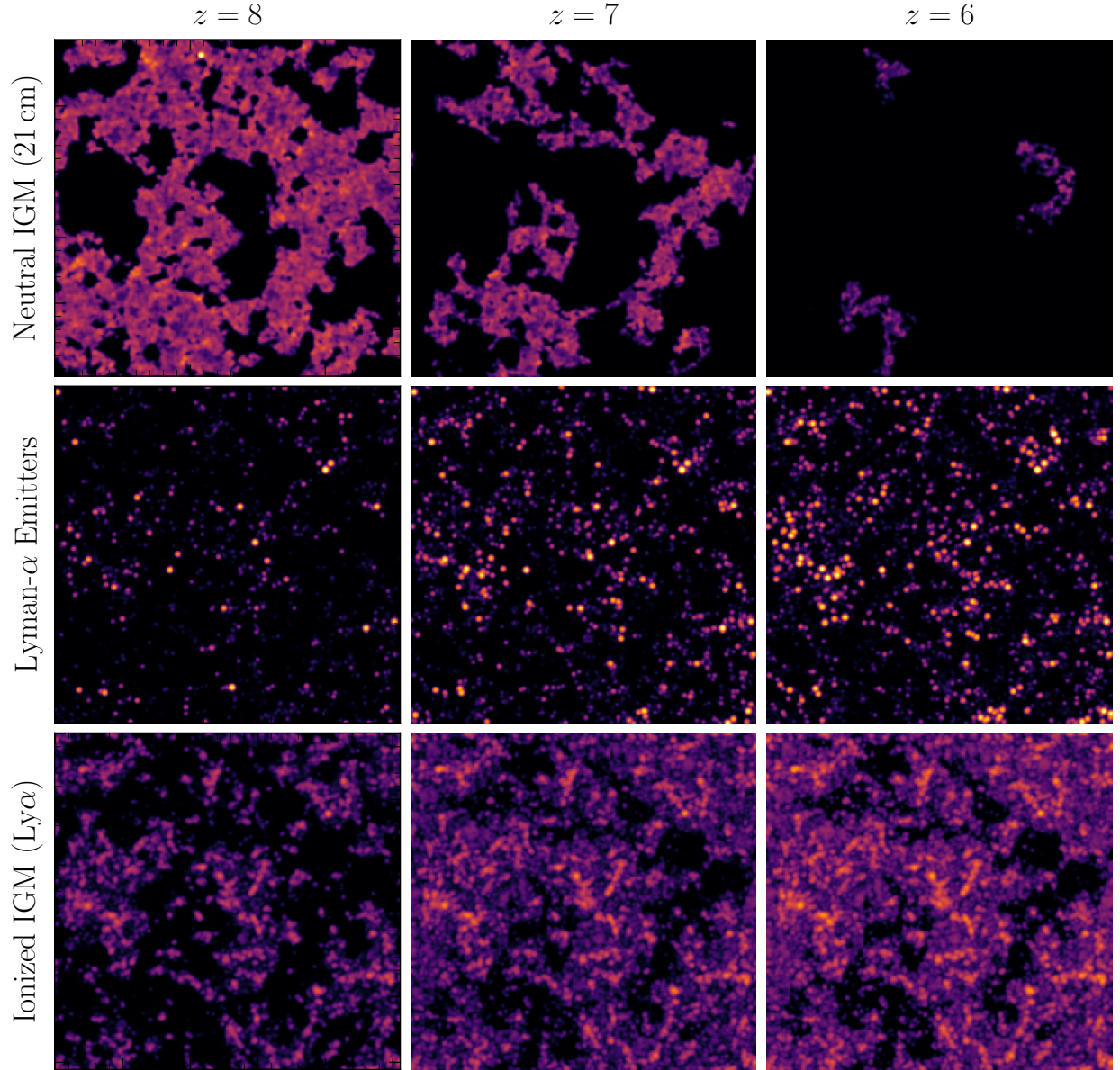


**Figure 7.** Slices through the simulated 21 cm brightness temperature offset,  $\delta T_b$ , and Ly $\alpha$  cubes.

### 2.2.3 Ly $\alpha$ Attenuation

$$L_{\text{obs}}^{\text{gal}} = L^{\text{gal}} e^{-\tau_{\text{Ly}\alpha}} \quad (18)$$

$$\tau_s \approx 6.45 \times 10^5 \left( \frac{\Omega_b h}{0.03} \right) \left( \frac{\Omega_m}{0.3} \right)^{-0.5} \left( \frac{1+z_s}{10} \right)^{1.5} \quad (19)$$

$$\begin{aligned} \tau_{\text{Ly}\alpha} &= \tau_s \bar{x}_{\text{HI}} \left( \frac{2.02 \times 10^{-8}}{\pi} \right) \left( \frac{1+z_s}{1+z_{\text{obs}}} \right)^{1.5} \\ &\times \left[ I \left( \frac{1+z_s}{1+z_{\text{obs}}} \right) - I \left( \frac{1+z_{\text{reion}}}{1+z_{\text{obs}}} \right) \right] \end{aligned} \quad (20)$$

$$\begin{aligned} I(x) &= \frac{x^{4.5}}{1-x} + \frac{9}{7}x^{3.5} + \frac{9}{5}x^{2.5} + 3x^{1.5} + 9x^{0.5} \\ &- 4.5 \log \left( \frac{1+x^{0.5}}{1-x^{0.5}} \right) \end{aligned} \quad (21)$$

### 3. Cross-Correlation Studies

Talk about the power spectrum and cross-power spectrum here.

#### 3.1. Cross-Power Spectrum

$$\langle \tilde{\delta}(\mathbf{k})\tilde{\delta}(\mathbf{k}') \rangle = (2\pi)^3 \delta_D(\mathbf{k} - \mathbf{k}') P(\mathbf{k}) \quad (22)$$

We can estimate the power spectrum with the relational

$$P(k) \approx \frac{\sum_{\mathbf{k} \in k} \langle |\tilde{\delta}(\mathbf{k})|^2 \rangle}{N_k V} \quad (23)$$

$$\tilde{\Delta}^2(k) = \frac{k^3}{2\pi^2} P(k) \quad (24)$$

$$\Delta_{\text{Ly}\alpha}^2(k) = (\nu \bar{I}_\nu)^2 \tilde{\Delta}_{\text{Ly}\alpha}^2(k) \quad (25)$$

$$\Delta_{21}^2(k) = (\delta \bar{T}_b)^2 \tilde{\Delta}_{21}^2(k) \quad (26)$$

$$\Delta_{21,\text{Ly}\alpha}^2(k) = (\delta \bar{T}_b)(\nu \bar{I}_\nu) \tilde{\Delta}_{21,\text{Ly}\alpha}^2(k) \quad (27)$$

$$r(k) = \frac{\Delta_{21,\text{Ly}\alpha}^2(k)}{\sqrt{\Delta_{21}^2(k) \Delta_{\text{Ly}\alpha}^2(k)}} \quad (28)$$

#### 3.2. Observational Uncertainties

To estimate the feasibility of making a measurement of the 21cm-Ly $\alpha$ cross-power spectrum, it is important to define the sources of error

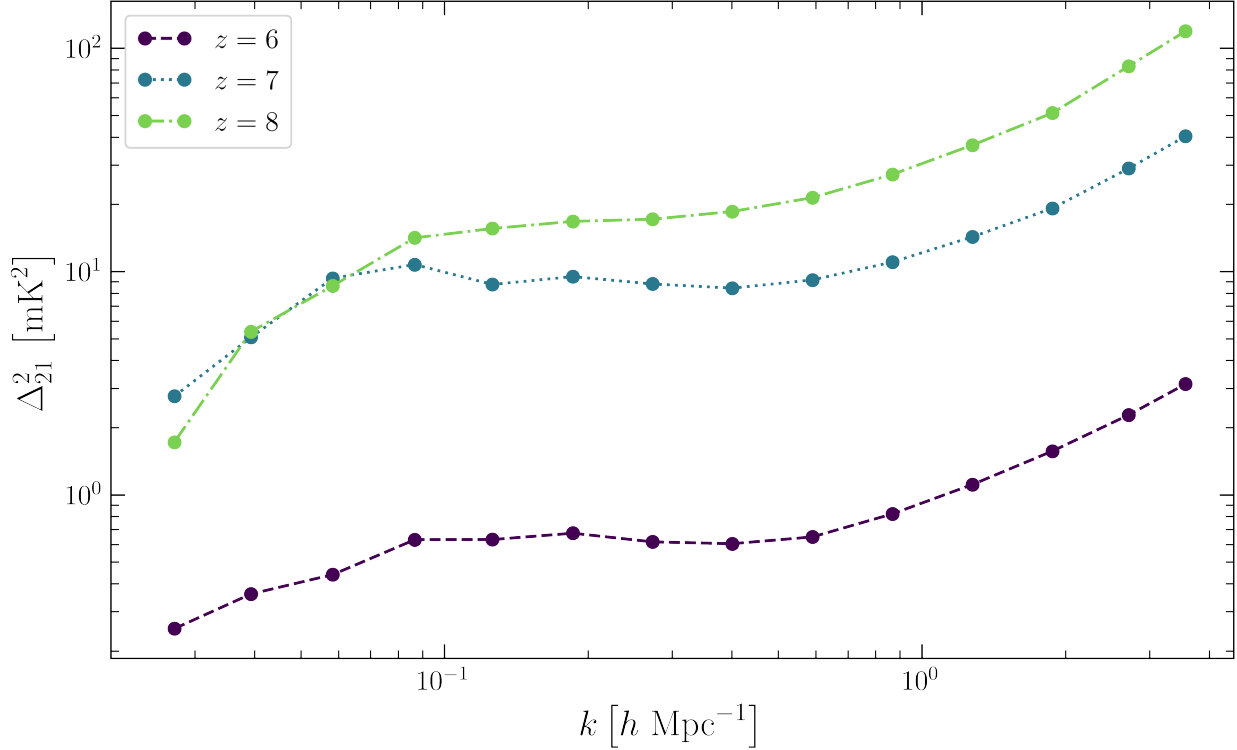


**Figure 8.** 21 cm power spectra plotted as a function of redshift for the fiducial 21cmFAST model.

$$\sigma_{21}(k) = [P_{21}(k) + P_{21,N}(k)] \quad (29)$$

$$P_{21,N} = X^2 Y \frac{T_{\text{sys}}^2}{2t} \frac{\Omega_p^2}{\Omega_{\text{pp}}} \quad (30)$$

Ly $\alpha$  uncertainty

$$\sigma_{\text{Ly}\alpha} = [P_{\text{Ly}\alpha} + P_{\text{Ly}\alpha,N}] \quad (31)$$

$$P_{\text{Ly}\alpha,N} = \sigma_N^2 V_{\text{vox}} W_{\text{Ly}\alpha}(k_\perp, k_\parallel) \quad (32)$$

$$W_{\text{Ly}\alpha}(k_\perp, k_\parallel) = \exp \left( \left( k_\perp / k_{\perp,\text{res}} \right)^2 + \left( k_\parallel / k_{\parallel,\text{res}} \right)^2 \right) \quad (33)$$

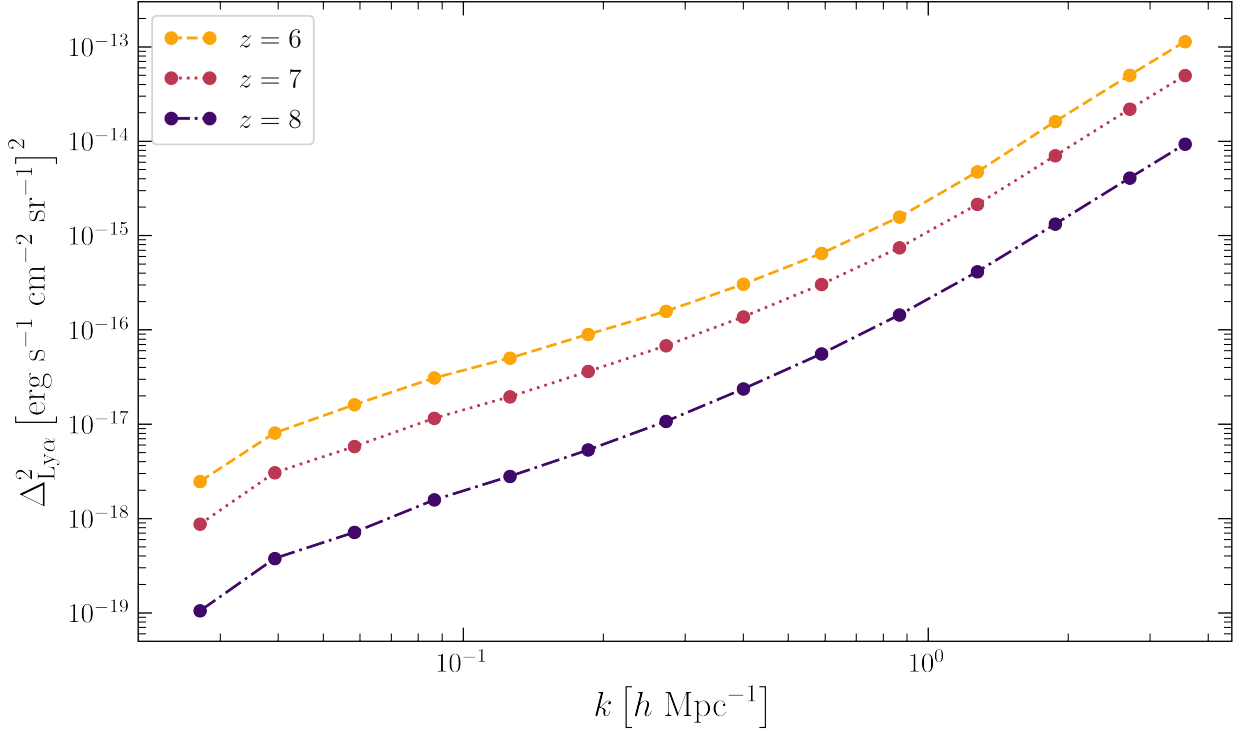


**Figure 9.** Ly $\alpha$  power spectra plotted for the redshift range of interest. Here, we include the Ly $\alpha$  contributions from both LAE's and the ionized IGM.

$$V_{\text{vox}} = A_{\text{pix}} r_{\text{pix}}$$

21cm-Ly $\alpha$  uncertainty

$$\sigma_{21, \text{Ly}\alpha}^2 = \frac{1}{2} [P_{21, \text{Ly}\alpha}^2 + \sigma_{21} \sigma_{\text{Ly}\alpha}] \quad (34)$$

### 3.3. Foreground Contamination

Here is an explanation of the wedge ([Datta et al. \(2010\)](#), [Morales et al. \(2012\)](#))

Cross-correlation of reionization-era 21 cm observations with Ly $\alpha$  intensity mapping surveys have the advantage that 21 cm foregrounds have no correlation with low redshift interloper lines. Because the two do not correlate, no power from the foregrounds is added to the cross-power spectrum. However, while the foregrounds don't contribute to the total cross-power spectrum, they do contribute to the overall variance of the measurement, and therefore the errors.

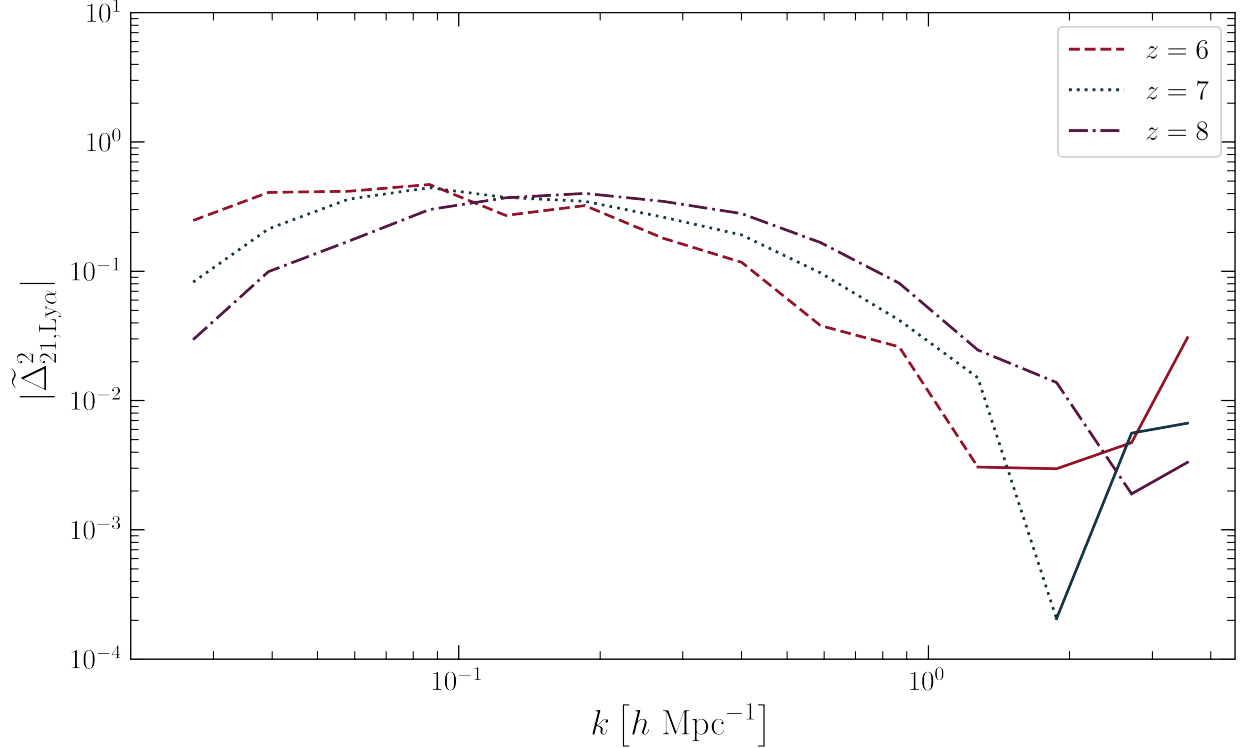


**Figure 10.** The dimensionless 21 cm-Ly $\alpha$  cross-power spectrum. The solid lines on each of the curves represent positive values in the cross-power spectrum, while varying line styles on the same curves represent negative values. As expected, the cross-power spectrum turns over from positive to negative on the scale of the mean ionized bubble size at that redshift. We also find the cross-power spectrum turns over at increasing scales as reionization progresses, tracing the growth of ionized bubbles.

$$k_{\parallel} \approx \theta_0 k_{\perp} \frac{D_M(z)}{D_H} \frac{E(z)}{(1+z)} \quad (35)$$

In the previous section, I calculated the cross-power spectrum for the case where foregrounds are completely uncorrelated (don't contribute to the cross-power spectrum amplitude) and where they did not contribute to the total variance. In this section, I'll take a more realistic and honest approach to calculating the errors by dealing with the 21 cm foregrounds in two different ways. There are two primary methods that I chose to deal with the foregrounds: by relying on the fact that the foregrounds are spectrally smooth and thus confined to an area of the 2D power spectrum known as the wedge and by assuming some

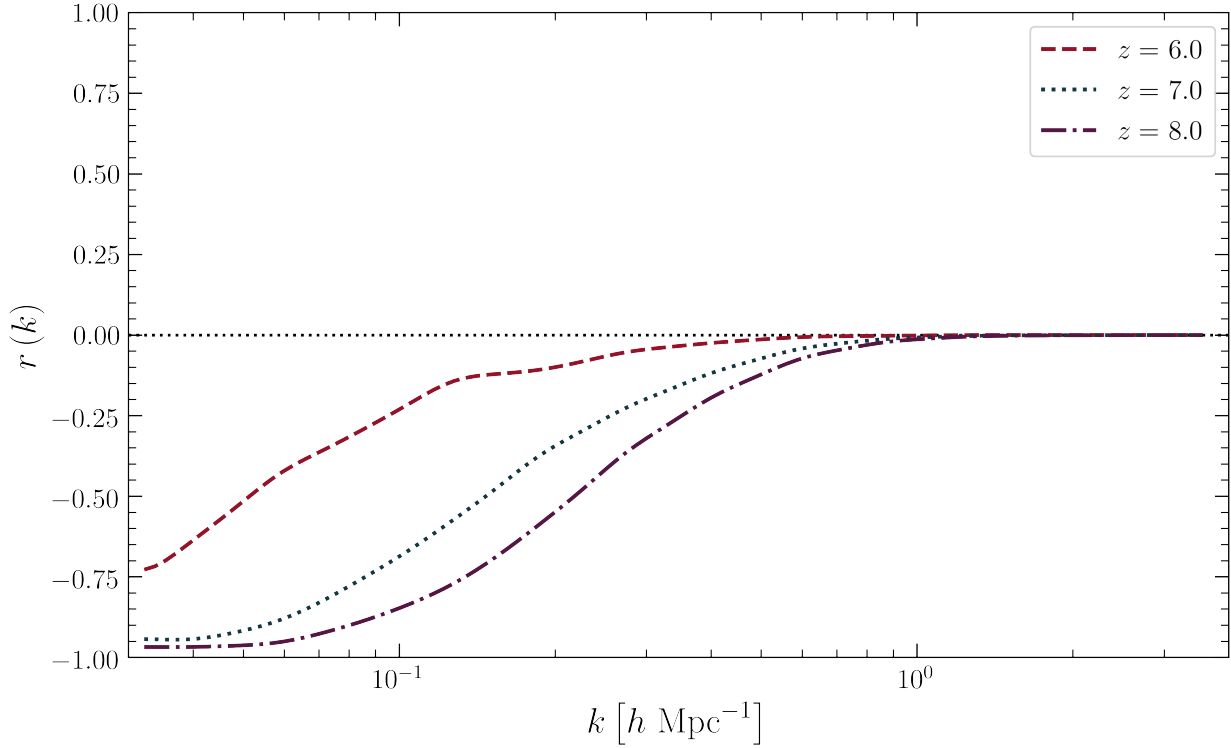


**Figure 11.** The cross-correlation coefficient plotted as a function of scale.

imperfect removal method. Each method has advantages and disadvantages.

In addition to avoiding 21 cm foregrounds by cutting out  $k$ -modes that fall within the wedge, efforts are being made to model galactic diffuse emission and extragalactic point sources to directly remove them from the data. This technique is known as foreground subtraction. While this modeling foregrounds accurately has been shown to be quite difficult, it gives the added benefit of recovering the foreground modes that fall within the wedge, increasing the signal to noise of the measurement at large scales, assuming perfect (or near perfect) foreground subtraction.

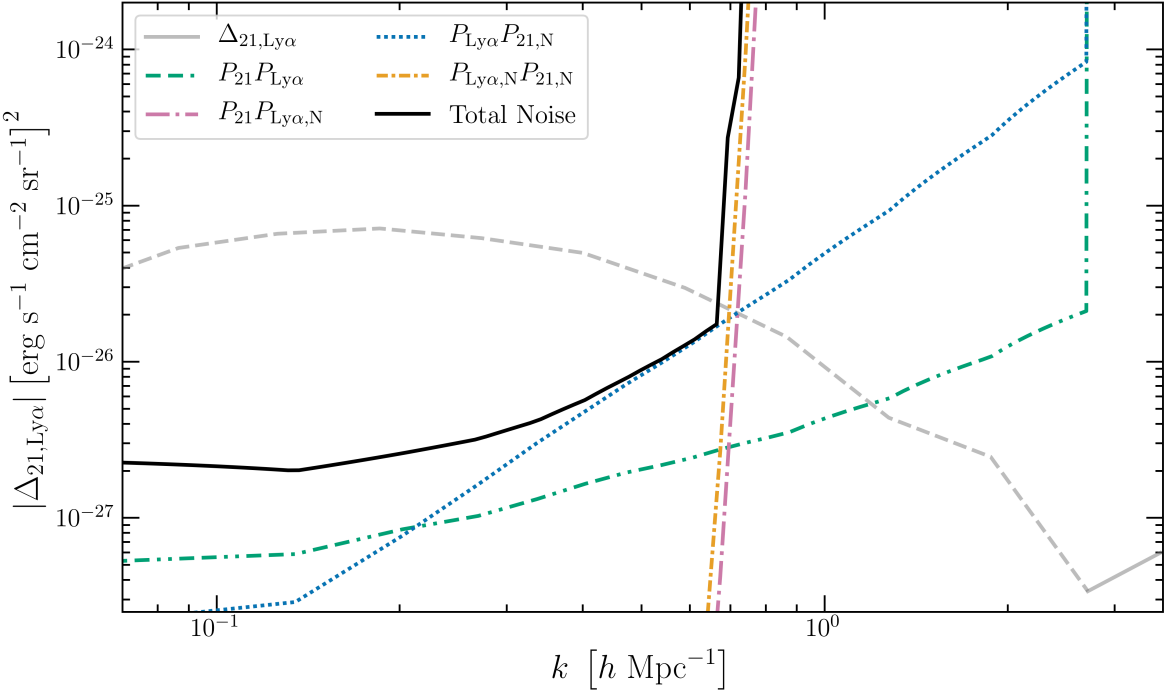
While outside the scope of this particular project, foreground subtraction could be a viable method for recovering  $k$ -modes dominated by bright 21 cm foregrounds and potentially allow for higher signal to noise measurements of the cross-power spectrum, given sufficient subtraction. In the case where 21 cm are avoided via subtraction of the wedge, the total variance on the 21 cm-Ly $\alpha$  cross power spectrum measurements would then be written as:

Table 1: Observing parameters for uncertainty calculations

HERA Observing Parameters	
Observing Days	180
Time Per Day (hrs)	6
Bandwidth (MHz)	8
Dish Size (m)	14
Number of Elements	320
$T_{\text{sys}}$	$100 + 120(\nu/150 \text{ MHz})^{-2.55} \text{ K}$
SPHEREx Observing Parameters	
$x_{\text{pix}} (\text{''})$	6.2
$\sigma_N [\text{erg s}^{-1} \text{ cm}^{-2} \text{ sr}^{-1}]$	$3 \times 10^{-20}$
$V_{\text{vox}} (\text{Mpc}^3)$	0.3
$R_{\text{res}}$	41.5

$$\sigma_{21,\text{Ly}\alpha}^2 = \frac{1}{2} \left[ P_{21,\text{Ly}\alpha}^2 + (P_{21} + P_{21,N} + P_{21,F}) (P_{\text{Ly}\alpha} + P_{\text{Ly}\alpha,N}) \right] \quad (36)$$

where  $P_{21,F}$  is the power spectrum due to foregrounds.



**Figure 12.** Error budgets of the sensitivity on the cross-power spectrum as measured by HERA and SPHEREx at  $z = 8$ . The terms  $P_{21,N}$  and  $P_{Ly\alpha,N}$  represent the thermal noise variance from HERA and SPHEREx respectively. Here, I neglect plotting the cross-power sample variance term,  $P_{21,Ly\alpha}$  as its contribution is negligible, however, it is represented in the total noise of the measurement. For reference, the cross-power spectrum is plotted in gray.

## 4. Conclusions

Despite the efforts of first-generation 21-cm experiments, the Epoch of Reionization remains one of the most mysterious periods in the universe’s history. Next-generation intensity mapping experiments, such as HERA and SPHEREx, look to shed light on this largely unexplored period. While each instrument should allow for an in-depth study of reionization, synergies between instruments like these will offer independent confirmation on reionization era physics and provide insight on the evolution of the first luminous sources.

While this was a decent proof of concept, a number of potential avenues have the oppor-

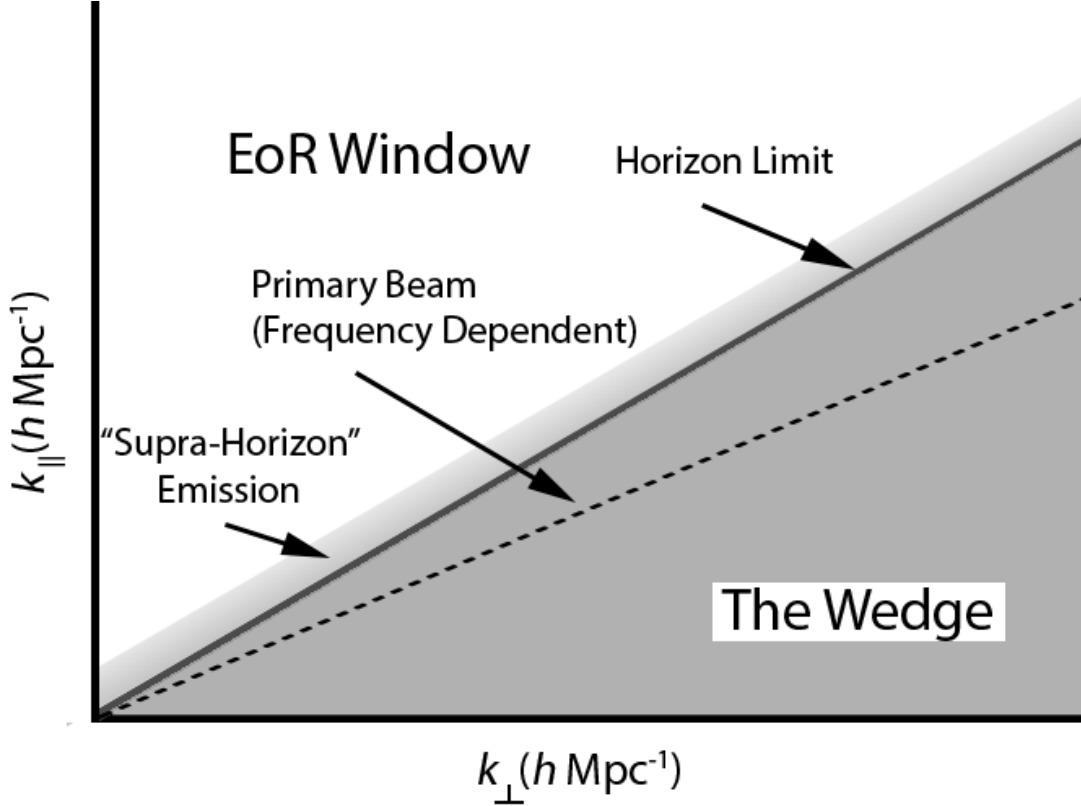


**Figure 13.** A depiction of the cylindrically averaged 21 cm power spectrum divided into the EoR window and the Wedge. Power from spectrally smooth foregrounds dominate the cosmological 21 cm signal at low  $k_{\parallel}$  values and bleed into higher  $k_{\parallel}$  modes the further they are from the field center, extending all the way to the horizon in cases of zenith-pointing telescopes such as HERA.

tunity to be explored in future work. This section BLAH, we provided a treatment of 21-cm foregrounds in which, we avoided the foreground dominated region in cylindrically averaged power spectrum by removing all modes within the foreground wedge. In the future, it might be interesting to explore other methods of foreground removal such as foreground subtraction. While it is likely that even optimistic levels of foreground modeling and subtraction (99.9% [Barry et al. \(2019\)](#)), would dominate the error budget of the cross-power spectrum, the relatively low noise contribution from SPHEREx may allow the cross-power spectrum to be detectable even in cases of imperfect foreground removal. In addition to an enhanced 21-cm foreground treatment, we ignored infrared foreground removal (CITE PIXEL MASKING SPHEREx PAPER). This likely will not significantly change the amplitude of the cross-power

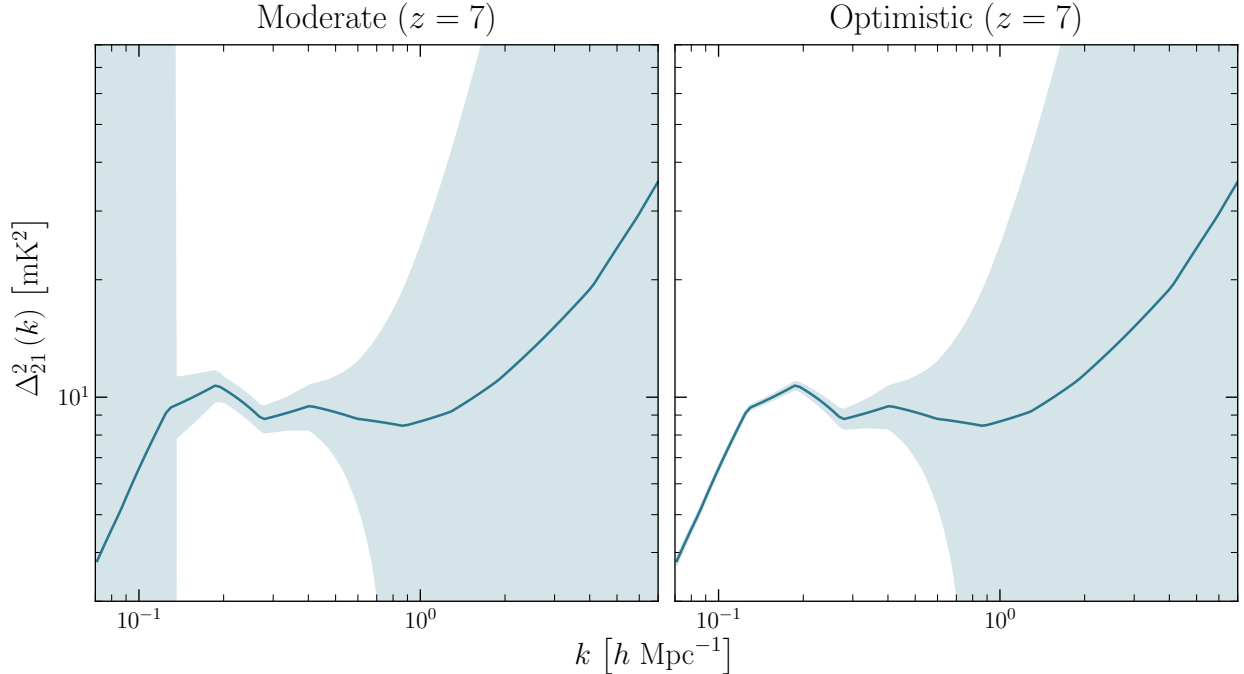


**Figure 14.** The 21 cm power spectrum plotted with  $1\sigma$  errors given observing parameters stated in table BLAH. Here, I compare the dependence of the two foreground cases on the noise. For the moderate case, all  $k$ -modes within the horizon limit are removed resulting in a complete loss of information on large scales  $k \lesssim 0.15 h \text{Mpc}^{-1}$ . For the optimistic case, foregrounds extend to the first null in HERA’s beam resulting in a much higher recovery of large scale information.

spectrum but could be added for completeness.

In spite of the fact that the cross-power spectrum turnover will remain undetectable by HERA and SPHEREx measurements, given the observational parameters that were chosen, this detection may still allow for constraints on cosmological and astrophysical parameters. In future work, we would like to quantify the accuracy with which the 21cm-Ly $\alpha$ cross-power spectrum can allow us to estimate cosmological parameters. This analysis has been done with the

In addition to Ly $\alpha$ , 21-cm measurements made by HERA will prove to be complementary to intensity mapping measurements of other spectral lines. In particular, instruments measuring the CO(2-1) rotational line (COMAP) and the CII fine structure line (TIME, CCAT-p, and CONCERTO) will be prime candidates for cross-correlation with HERA in the

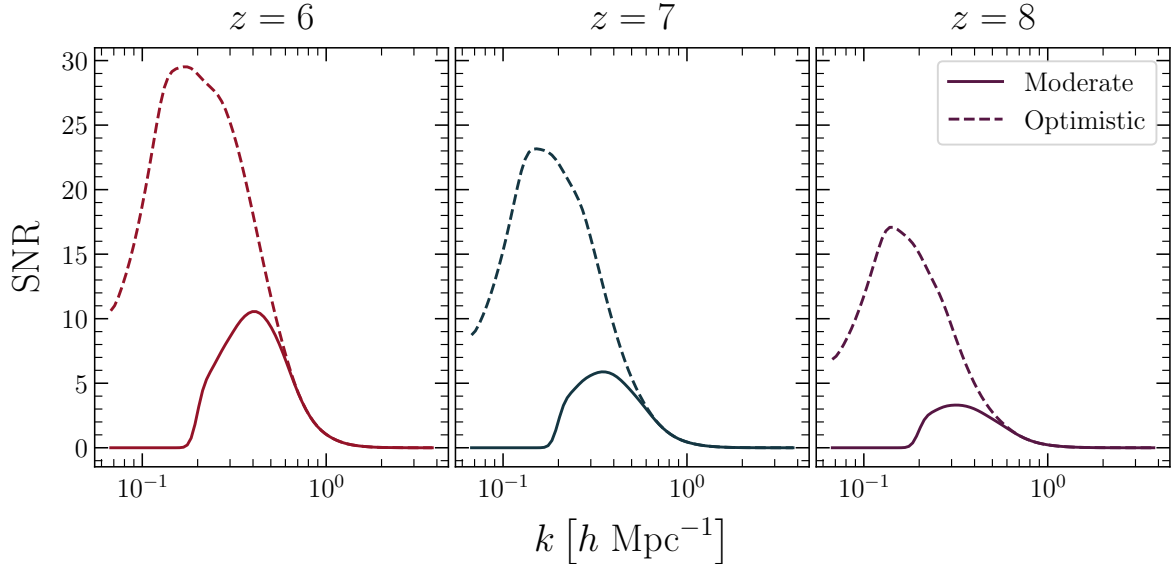


**Figure 15.** Signal to noise estimates for the 21cm-Ly $\alpha$  cross-power spectrum. The redshifts  $z = [6, 7, 8]$  are plotted for both the optimistic and moderate foreground treatments. These estimates take into account the 21cm foreground wedge, thermal and sample variance from HERA and SPHEREx, and Ly $\alpha$  attenuation due to absorption in the neutral IGM.

near future, as the 21-CO and 21-CII cross-power spectra are expected to have a similar anti-correlation as the 21-Ly $\alpha$  cross-power spectrum. One possible extension of this work could be to model intensity mapping from these lines during the EoR using 21cmFASTcubes and estimate the feasibility of HERA of cross-correlating with these experiments. If the 21cm-CO or 21cm-CII cross-power spectrum proves to be measurable, they should each provide additional confirmation of an EoR detection and give insight into ionized bubble size and mean ionization fraction.

# References

- Barry, N., Wilensky, M., Trott, C. M., et al. 2019, ApJ, 884, 1, doi: [10.3847/1538-4357/ab40a8](https://doi.org/10.3847/1538-4357/ab40a8)
- Chang, T. C., Gong, Y., Santos, M., et al. 2015, in Advancing Astrophysics with the Square Kilometre Array (AASKA14), 4
- Comaschi, P., Yue, B., & Ferrara, A. 2016, MNRAS, 463, 3193, doi: [10.1093/mnras/stw2198](https://doi.org/10.1093/mnras/stw2198)
- Datta, A., Bowman, J. D., & Carilli, C. L. 2010, ApJ, 724, 526, doi: [10.1088/0004-637X/724/1/526](https://doi.org/10.1088/0004-637X/724/1/526)
- DeBoer, D. R., Parsons, A. R., Aguirre, J. E., et al. 2017, PASP, 129, 045001, doi: [10.1088/1538-3873/129/974/045001](https://doi.org/10.1088/1538-3873/129/974/045001)
- Doré, O., Bock, J., Ashby, M., et al. 2014, arXiv e-prints, arXiv:1412.4872. <https://arxiv.org/abs/1412.4872>
- Feng, C., Cooray, A., & Keating, B. 2017, ApJ, 846, 21, doi: [10.3847/1538-4357/aa7ff1](https://doi.org/10.3847/1538-4357/aa7ff1)
- Furlanetto, S. R., & Lidz, A. 2007, ApJ, 660, 1030, doi: [10.1086/513009](https://doi.org/10.1086/513009)
- Gong, Y., Silva, M., Cooray, A., & Santos, M. G. 2014, ApJ, 785, 72, doi: [10.1088/0004-637X/785/1/72](https://doi.org/10.1088/0004-637X/785/1/72)
- Heneka, C., Cooray, A., & Feng, C. 2017, ApJ, 848, 52, doi: [10.3847/1538-4357/aa8eed](https://doi.org/10.3847/1538-4357/aa8eed)
- Hutter, A., Dayal, P., Müller, V., & Trott, C. M. 2017, ApJ, 836, 176, doi: [10.3847/1538-4357/836/2/176](https://doi.org/10.3847/1538-4357/836/2/176)
- Hutter, A., Dayal, P., Partl, A. M., & Müller, V. 2014, MNRAS, 441, 2861, doi: [10.1093/mnras/stu791](https://doi.org/10.1093/mnras/stu791)

- Kubota, K., Inoue, A. K., Hasegawa, K., & Takahashi, K. 2019, arXiv e-prints, arXiv:1910.02361. <https://arxiv.org/abs/1910.02361>
- Kubota, K., Yoshiura, S., Takahashi, K., et al. 2018, MNRAS, 479, 2754, doi: [10.1093/mnras/sty1471](https://doi.org/10.1093/mnras/sty1471)
- Liu, A., & Shaw, J. R. 2019, arXiv e-prints, arXiv:1907.08211. <https://arxiv.org/abs/1907.08211>
- Mesinger, A., Furlanetto, S., & Cen, R. 2011, MNRAS, 411, 955, doi: [10.1111/j.1365-2966.2010.17731.x](https://doi.org/10.1111/j.1365-2966.2010.17731.x)
- Morales, M. F., Hazelton, B., Sullivan, I., & Beardsley, A. 2012, ApJ, 752, 137, doi: [10.1088/0004-637X/752/2/137](https://doi.org/10.1088/0004-637X/752/2/137)
- Neben, A. R., Stalder, B., Hewitt, J. N., & Tonry, J. L. 2017, ApJ, 849, 50, doi: [10.3847/1538-4357/aa8f9c](https://doi.org/10.3847/1538-4357/aa8f9c)
- Silva, M. B., Santos, M. G., Gong, Y., Cooray, A., & Bock, J. 2013, ApJ, 763, 132, doi: [10.1088/0004-637X/763/2/132](https://doi.org/10.1088/0004-637X/763/2/132)
- Silva, M. B., & Zaroubi, S. 2018, in IAU Symposium, Vol. 333, Peering towards Cosmic Dawn, ed. V. Jelić & T. van der Hulst, 250–253
- Sobacchi, E., Mesinger, A., & Greig, B. 2016, MNRAS, 459, 2741, doi: [10.1093/mnras/stw811](https://doi.org/10.1093/mnras/stw811)

# Appendix

This is where appendix-y things go